Detonations in sub-chandrasekhar-mass C+O white dwarfs

The Astrophysical Journal Letters, 714:L52–L57, 2010 May 1 doi:10.1088/2041-8205/714/1/L52

DETONATIONS IN SUB-CHANDRASEKHAR-MASS C+O WHITE DWARFS

S. A. Sim, F. K. Röpke, W. Hillebrandt, M. Kromer, R. Pakmor, M. Fink, A. J. Ruiter, and I. R. Seitenzahl
Max-Planck-Institut für Astrophysik, Karl-Schwarzschild-Str. 1, D-85748 Garching, Germany
Received 2009 December 22; accepted 2010 March 11; published 2010 April 1

ABSTRACT

Explosions of sub-Chandrasekhar-mass white dwarfs (WDs) are one alternative to the standard Chandrasekhar-mass model of Type Ia supernovae (SNe Ia). They are interesting since binary systems with sub-Chandrasekhar-mass primary WDs should be common and this scenario would suggest a simple physical parameter which determines the explosion brightness, namely the mass of the exploding WD. Here we perform one-dimensional hydrodynamical simulations, associated post-processing nucleosynthesis, and multi-wavelength radiation transport calculations for pure detonations of carbon–oxygen WDs. The light curves and spectra we obtain from these simulations are in good agreement with observed properties of SNe Ia. In particular, for WD masses from 0.97 to 1.15 $M_{\odot}$ we obtain ^{56}Ni masses between 0.3 and 0.8 $M_{\odot}$, sufficient to capture almost the complete range of SN Ia brightnesses. Our optical light curve rise times, peak colors, and decline timescales display trends which are generally consistent with observed characteristics although the range of *B*-band decline timescales displayed by our current set of models is somewhat too narrow. In agreement with observations, the maximum light spectra of the models show clear features associated with intermediate-mass elements and reproduce the sense of the observed correlation between explosion luminosity and the ratio of the Si II lines at λ6355 and λ5972. We therefore suggest that sub-Chandrasekhar-mass explosions are a viable model for SNe Ia for any binary evolution scenario leading to explosions in which the optical display is dominated by the material produced in a detonation of the primary WD.

Key words: radiative transfer – supernovae: general – white dwarfs

1. INTRODUCTION

In recent years, considerable work has been devoted to the study of the Chandrasekhar-mass ($M_{\rm Ch}$) model of Type Ia supernovae (SNe Ia). As shown by Arnett et al. (1971), prompt detonations of $M_{\rm Ch}$ carbon/oxygen (C+O) white dwarfs (WDs) in hydrostatic equilibrium mainly produce iron group elements (IGEs). Thus, they cannot account for the significant amounts of intermediate-mass elements (IMEs; e.g., silicon and sulfur) responsible for the features which dominate the maximum light spectra. To obtain these, pre-expansion of the WD is necessary such that burning partially takes place under low-density conditions where IMEs can be synthesized. One way of achieving this is provided by models in which the flame ignites as a deflagration which releases sufficient energy to expand the star before a deflagration-to-detonation transition occurs (Khokhlov 1991). An alternative to this pre-expansion is the detonation of a sub-Chandrasekhar-mass (sub-$M_{\rm Ch}$) WD starting from a hydrostatic configuration. Here, a variety of density profiles can be realized, determined by the WD mass. Close to $M_{\rm Ch}$, the detonation produces primarily IGEs and few IMEs, while for less massive WDs more IMEs and less IGEs will be synthesized.

Detonation of a sub-$M_{\rm Ch}$ WD cannot occur spontaneously but must be triggered by external compression. The most widely discussed mechanism for sub-$M_{\rm Ch}$ explosions has been the *double-detonation* model. Here, a C+O WD accretes from a companion star and develops a helium-rich outer shell. This may occur for binaries with helium-rich donors or hydrogen-rich donors where the accreted hydrogen is burned to helium. If the helium shell becomes sufficiently massive, it can become unstable and detonate. Subsequent compression of the core by inward propagating shocks may produce a secondary carbon detonation which explodes the WD (e.g., Woosley & Weaver 1986; Fink et al. 2007). Detonations in helium-rich surface layers have also been discussed for the case of rapid dynamical mass transfer in binary systems containing a C+O WD with a helium-rich WD companion (Guillochon et al. 2010). In that case instabilities in the accretion seed dense knots which, by impacting on the underlying WD surface, might trigger a detonation in the accreted helium leading to a potential secondary core detonation. It has also been speculated that sub-$M_{\rm Ch}$ explosions may arise during violent accretion in mergers of C+O WD binaries. Here, the C+O accretion may lead to an edge-lit detonation or carbon flashes that trigger a core detonation (see, e.g., Shigeyama et al. 1992, but for a different result see Lorén-Aguilar et al. 2009).

Most previous work on testing sub-$M_{\rm Ch}$ models has focused on cases in which the core detonation is triggered by detonation in an overlying massive shell ($\sim$0.2 $M_{\odot}$) of helium (e.g., Woosley & Weaver 1994; Livne & Arnett 1995; Höflich & Khokhlov 1996; Höflich et al. 1996; Nugent et al. 1997). In those models burning in the helium shell synthesizes significant masses of ^{56}Ni in the outer ejecta, leading to spectra and light curves in conflict with observations. As noted in those studies, however, these conclusions are strongly dependent on the influence of the shell material. In particular, they may not be applicable if such a layer is absent (or much less massive) or if its post-burning composition lacks ^{56}Ni. Recently, Bildsten et al. (2007) suggested that detonation of the helium shell may be possible for a shell with mass as low as $\sim$0.055 $M_{\odot}$ around a 1.025 $M_{\odot}$ C+O core and that the burning produces only 0.012 $M_{\odot}$ of ^{56}Ni along with some lighter IGEs (Guillochon et al. 2010 find that even lower atomic-number burning products can dominate in their helium detonations). Even for the low shell masses of Bildsten et al. (2007), Fink et al. (2010) find that a secondary core detonation is possible. To date, sub-$M_{\rm Ch}$ explosions in the absence of a nickel-rich outer layer have not been studied in detail. Shigeyama et al. (1992) investigated the explosion dynamics of sub-$M_{\rm Ch}$ detonations and concluded that

Table 1
Nucleosynthesis Products and Optical Light Curve Properties[a] for Detonations of White Dwarfs

Parameter	Models					
$M_{\rm WD}^{\rm b}$ ($M_\odot$)	1.15	1.06	1.06	0.97	0.88	0.81
$\rho_{\rm c}^{\rm c}$ (g cm^{-3})	7.9×10^7	4.15×10^7	4.15×10^7	2.4×10^7	1.45×10^7	1.0×10^7
WD comp. (C/O/Ne)[d]	50/50/0	50/50/0	42.5/50/7.5	50/50/0	50/50/0	50/50/0
$E_{\rm nuc}$[e] (foe)	1.64	1.41	1.41	1.19	0.97	0.82
$E_{\rm k}$[e] (foe)	1.39	1.22	1.22	1.04	0.86	0.73
Cell size[f] (cm)	1.0×10^6	1.1×10^6	1.1×10^6	1.3×10^6	1.5×10^6	1.7×10^6
$M_{^{56}\rm Ni}$[g] ($M_\odot$)	0.81	0.56	0.43	0.30	0.07	0.01
$M_{\rm IGE}$[g] ($M_\odot$)	2.1×10^{-2}	1.7×10^{-2}	1.8×10^{-1}	1.2×10^{-2}	4.7×10^{-3}	8.7×10^{-4}
$M_{\rm IME}$[g] ($M_\odot$)	0.27	0.41	0.36	0.54	0.63	0.57
$M_{\rm O}$[g] ($M_\odot$)	0.04	0.08	0.09	0.12	0.17	0.22
Δm_{15} (mag)	1.34	1.56	1.42	1.73	1.77	...
$t_{\rm max}^{\rm B}$ (mag)	19.2	20.1	18.0	19.9	14.1	...
$B_{\rm max}$[h] (mag)	−19.9	−19.2	−18.7	−18.5	−16.6	...
$V_{\rm max}$[h] (mag)	−19.6	−19.4	−19.3	−18.8	−17.3	...
$R_{\rm max}$[h] (mag)	−19.8	−19.3	−19.3	−18.8	−17.7	...
$I_{\rm max}$[h] (mag)	−19.6	−19.0	−19.2	−18.7	−17.8	...
$(B-V)_{\rm max}$[h] (mag)	0.15	0.13	0.48	0.24	0.63	...
$v_{\rm Si\,II}$[i] (km s^{-1})	12500	11500	11500	9000	6000	...

Notes.
[a] Since it has very low ^{56}Ni mass, we did not perform radiative transfer simulations for the 0.81 $M_\odot$ model.
[b] Mass of white dwarf.
[c] Central density of white dwarf.
[d] Initial composition of WD (percentage by mass of ^{12}C/^{16}O/^{22}Ne).
[e] Energy released by nuclear burning ($E_{\rm nuc}$) and asymptotic kinetic energy of the ejecta ($E_{\rm k}$).
[f] Initial size of computational grid cells in the WD. Since the simulations use an expanding grid, the physical resolution degrades with time.
[g] Mass yields for ^{56}Ni, stable iron group elements (IGEs), intermediate-mass elements (IMEs), and oxygen (O).
[h] Peak magnitudes are given at the true peaks in each band. Colors are quoted at time ($t_{\rm max}^{\rm B}$) of the B-band maximum.
[i] Blueshift velocity of Si II λ6355 at $t_{\rm max}^{\rm B}$.

their characteristic properties were consistent with SNe Ia but they did not perform realistic radiative transfer simulations.

A full treatment of any class of sub-$M_{\rm Ch}$ explosion model requires realistic hydrodynamical and nucleosynthesis simulations of the accretion phase, triggering mechanism, and subsequent explosion. Here, however, we present a simple numerical experiment that is relevant to any class of sub-$M_{\rm Ch}$ explosion model. We consider pure detonations of sub-$M_{\rm Ch}$ C+O WDs with different masses, neglecting the question of how this detonation is initiated. This allows us to investigate the idealized case of sub-$M_{\rm Ch}$ detonation scenarios in which the observable display is dominated by material produced in the core explosion. Our goal is to determine the extent to which the least ambiguous component of the system, namely the detonation of a sub-$M_{\rm Ch}$ C+O WD, could lead to explosions which are consistent with observations of SNe Ia.

2. HYDRODYNAMIC SIMULATIONS

To explore the properties of detonations of sub-$M_{\rm Ch}$ WDs, we set up five hydrostatic models with WD masses ($M_{\rm WD}$) ranging from 0.81 to 1.15 $M_\odot$ (see Table 1) with centrally ignited detonations. We performed the simulations in an axisymmetric setup of the full star but as the initial conditions were spherically symmetric and the symmetry is preserved during evolution, our models are one dimensional. The simulations were performed with our SNe Ia explosion code (the initial sizes of the computational grid cells are given in Table 1; see Fink et al. 2010 for technical details).

The detonations were represented with the level-set technique (Reinecke et al. 1999). This requires as inputs the detonation velocity and the energy release in the burning. The detonation velocities take into account pathological detonation speeds at high fuel densities (Gamezo et al. 1999), whereas low-density detonations are assumed to be of Chapman–Jouguet type (see Fink et al. 2010 for details). The energy released by nuclear burning ($E_{\rm nuc}$) and the asymptotic kinetic energy of the ejecta ($E_{\rm k}$) are given for each model in Table 1.

3. NUCLEOSYNTHESIS CALCULATIONS

The nucleosynthesis was computed using our standard tracer-particle technique (Travaglio et al. 2004). The masses obtained for ^{56}Ni, stable IGEs, IMEs, and O are given in Table 1.

We first computed nucleosynthesis for all five explosion simulations assuming an initial WD composition of uniformly mixed ^{12}C and ^{16}O with equal mass fractions ("pure-C+O," hereafter). Although commonly adopted in Type Ia explosion modeling, this composition is not strictly correct since the mass fraction of ^{16}O is expected to be larger than ^{12}C in the inner regions (e.g., Salaris et al. 1997). For $M_{\rm Ch}$ delayed-detonation models, Domínguez et al. (2001) showed that the C/O ratio affects the ^{56}Ni mass by ∼14% and the velocity structure of the ejecta by up to a few 1000 km s^{-1}. Our calculations are expected to have a similar sensitivity to the adopted C/O ratio. Moreover, C+O WDs formed from progenitors with non-zero metallicity will be polluted by some ^{22}Ne. Since the neutron excess of ^{22}Ne significantly affects the nucleosynthesis, for one of the hydrodynamical models ($M_{\rm WD}$ = 1.06 $M_\odot$) we repeated the nucleosynthesis post-processing step adopting a high initial ^{22}Ne mass fraction of 7.5% (this would correspond to a rather high-metallicity progenitor,

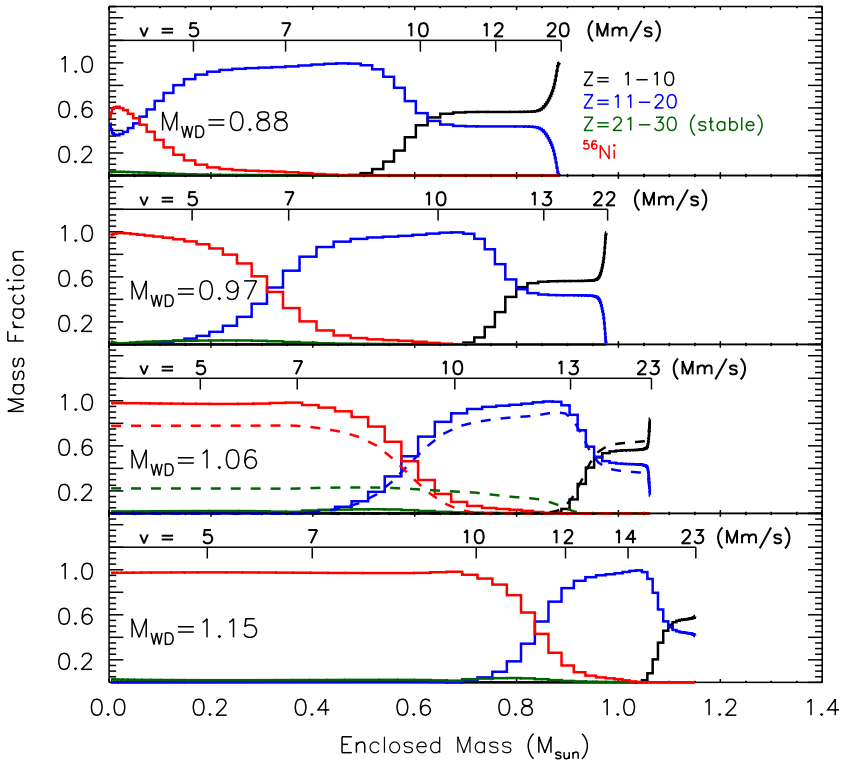

Figure 1. Composition vs. mass coordinate for the four models that produced significant masses of ^{56}Ni (least to most massive; top to bottom). The black histograms indicate low-mass elements and the blue shows IMEs (Z = 11–20). Red represents ^{56}Ni while stable IGEs (Z = 21–30) are shown in green. In the third panel the solid lines show the results for the pure-C+O model, while the dashed lines show the C+O+Ne model. In each panel, the velocity scale (in Mm s^{-1}) is also indicated.

$Z_0 \sim 3Z_\odot$). This model ("C+O+Ne," hereafter) allows us to bracket some of the systematic uncertainties associated with progenitor composition. The nucleosynthesis yields for this model are also given in Table 1.

The range of $M_{\rm WD}$ we consider leads to ^{56}Ni masses from $\sim$0.01 $M_\odot$ to 0.81 $M_\odot$, wide enough to encompass the range implied for all but the brightest SNe Ia (see, e.g., Stritzinger et al. 2006). The lowest mass models $M_{\rm WD}$ = 0.81 and 0.88 $M_\odot$ make very little ^{56}Ni ($\sim$0.01 and 0.07 $M_\odot$, respectively). Thus, they would be faint and lie outside the range of normal SNe Ia. Throughout the following, we therefore neglect further discussion of the $M_{\rm WD}$ = 0.81 $M_\odot$ model but retain the 0.88 $M_\odot$ model as a point of reference for the faintest observed SNe Ia.

Figure 1 shows the stratification of the nucleosynthesis products grouped into low-mass elements, IMEs, stable IGEs, and ^{56}Ni. The structure of the models is very similar to that obtained by Shigeyama et al. (1992): small masses of stable IGEs are produced and the mass shell in which large mass fractions of IMEs are produced is fairly extended. Significant IME mass fractions are present up to almost the highest velocities in all models, consistent with the lower limits on the outer extent of Si-rich material discussed by Mazzali et al. (2007). Moreover, a clear trend exists whereby the inner boundary of the IME-rich layers lies at higher velocities in the models where the ^{56}Ni mass is larger, the same trend as inferred from observations (Mazzali et al. 2007).

The most important consequence of ^{22}Ne in our C+O+Ne model is a substantial increase in the mass of stable IGEs (see Table 1 and the third panel of Figure 1; see also Höflich et al. 1998). These extend over a wide range of mass coordinate and come at the expense of less ^{56}Ni in the inner regions and fewer IMEs in the outer zones.

4. RADIATIVE TRANSFER SIMULATIONS

For each of the four detonation models that produce >0.05 $M_\odot$ of ^{56}Ni, we performed radiative transfer simulations using our Monte Carlo code ARTIS (Sim 2007; Kromer & Sim 2009). For $M_{\rm WD}$ = 1.06 $M_\odot$, we ran simulations for both our pure-C+O and C+O+Ne models. For all calculations, we used our largest atomic data set ($\sim 8.2 \times 10^6$ lines) and our non-LTE treatment of ionization (see Kromer & Sim 2009). Table 1 gives the light curve decline-rate parameter (Δm_{15}),[1] the time of B-band maximum light ($t^{\rm B}_{\rm max}$), the optical peak magnitudes, and the $B-V$ color at $t^{\rm B}_{\rm max}$.

5. COMPARISON WITH OBSERVATIONS

In Figure 2, we show the ultraviolet–optical–infrared (*UVOIR*) bolometric and the band-limited (U, B, V, R, I, J, H, and K bands) light curves from our radiative transfer simulations. Maximum light spectra are shown for the same calculations in Figure 3. Observations of two SNe Ia (SN 2005cf and SN 2004eo) are shown for comparison in both figures. The ^{56}Ni masses reported for these objects are significantly different but within the range covered by our models (0.45 $M_\odot$ for SN 2004eo, Pastorello et al. 2007a; 0.7 $M_\odot$ for SN 2005cf Pastorello et al. 2007b).

Given the simplicity of the underlying explosion simulations, the light curve shapes and colors are in remarkably good agreement with observations. For $M_{\rm WD}$ = 0.97, 1.06, and 1.15 $M_\odot$, we obtain B-band rise times of 18–20 days, close to observational estimates ($\sim$19 days; Conley et al. 2006). The peak colors are also close to those observed but slightly redder in

[1] Δm_{15} is defined as the change in B-band magnitude between maximum light and 15 days thereafter.

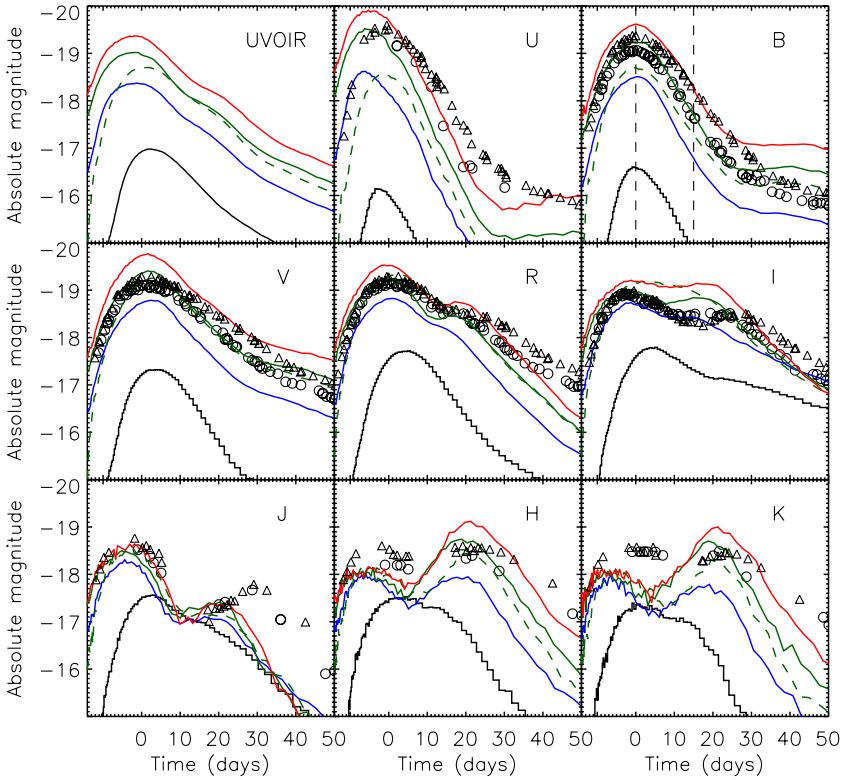

Figure 2. Computed *UVOIR* bolometric, *U*-, *B*-, *V*-, *R*-, *I*-, *J*-, *H*-, and *K*-band light curves for $M_{\rm WD} = 1.15$, 1.06, 0.97, and 0.88 $M_{\odot}$ (red, green, blue, and black, respectively). For $M_{\rm WD} = 1.06$ $M_{\odot}$, light curves for both our pure-C+O and C+O+Ne models are shown (solid and dashed green lines, respectively). Photometry for SN 2004eo (black circles; Pastorello et al. 2007a) and SN 2005cf (black triangles; Pastorello et al. 2007b) are also shown. The observations have been corrected for reddening and distance using parameters from Pastorello et al. (2007a, 2007b).

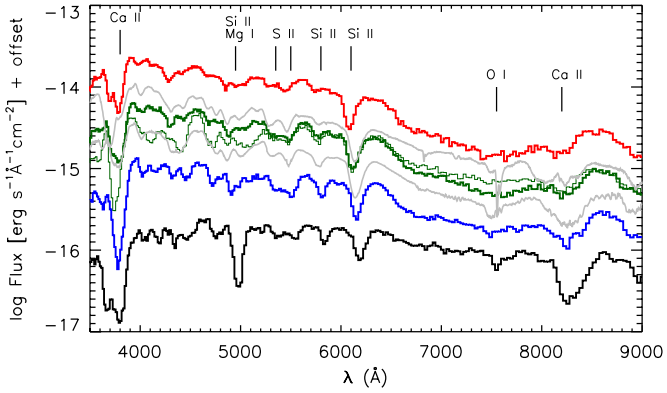

Figure 3. Computed spectra at *B*-band maximum light for $M_{\rm WD} = 1.15$, 1.06, 0.97, and 0.88 $M_{\odot}$ (red, green, blue, and black, respectively). For $M_{\rm WD} = 1.06$ $M_{\odot}$, spectra for both our pure-C+O and C+O+Ne models are shown (thick and thin green lines, respectively). Observed spectra of two SNe Ia around maximum light are shown for comparison: SN 2004eo (lower gray line; Pastorello et al. 2007a) and SN 2005cf (upper gray line; Garavini et al. 2007). Arbitrary vertical offsets have been applied for clarity. The observed spectra are de-redshifted and de-reddened using parameters from Pastorello et al. (2007a, 2007b).

$B-V$ compared to $M_{\rm Ch}$ models of similar brightness (compare with Höflich et al. 1996; Kasen et al. 2009). These results differ from previous studies for sub-$M_{\rm Ch}$ models where relatively rapid rise times (see, e.g., Höflich et al. 1996) and *blue* colors (see, e.g., Höflich et al. 1996; Nugent et al. 1997) were found. Both systematic differences arise due to significant amounts of ^{56}Ni present in the outer layers of their models (see discussion by Höflich & Khokhlov 1996). Thus, our calculations illustrate that *if* core detonations can be triggered *without* producing large masses of IGEs in the outer layers then good agreement with observations can be obtained. A modest additional mass of IMEs or unburned fuel (^{12}C, ^{16}O, or helium) in the outer ejecta due to the triggering mechanism would have minor consequences for the spectra.

Our maximum light spectra are also in qualitatively good agreement with observations (Figure 3). The models all show the characteristic Si II λ6355 feature. Moreover, they reproduce the sense of the observed trend whereby the strength of the weaker Si II feature at λ5972 relative to λ6355 is systematically smaller in brighter events (Nugent et al. 1995; Bongard et al. 2006; Hachinger et al. 2008). In agreement with observations, the maximum light spectra show clear features associated with other IMEs, in particular Ca and S. Our fainter models also predict O I absorption (λ7773) as observed in some SNe Ia (including SN 2004eo; see Figure 3) but this feature becomes weak for our brighter models, a trend also consistent with observations (Nugent et al. 1995). As expected from Figure 1, there is a tendency for higher velocities of IME features in brighter events. Velocities for Si II λ6355 measured from our spectra are given in Table 1 and are generally compatible with those inferred from observations (e.g., Benetti et al. 2005). The Si velocity for our pure-C+O $M_{\rm WD} = 1.06$ $M_{\odot}$ model is slightly too high for both SN 2004eo and SN 2005cf. However, this discrepancy is small and on the scale of the differences between the models (the observed line velocities are bracketed by those in our $M_{\rm WD} = 0.97$ and 1.06 $M_{\odot}$ maximum light spectra).

Figure 4 shows the *B*-band width–luminosity relationship obtained from our models compared with the properties of a sample of well-observed SNe Ia (Hicken et al. 2009). The models reproduce the correct systematic trend: brighter models have light

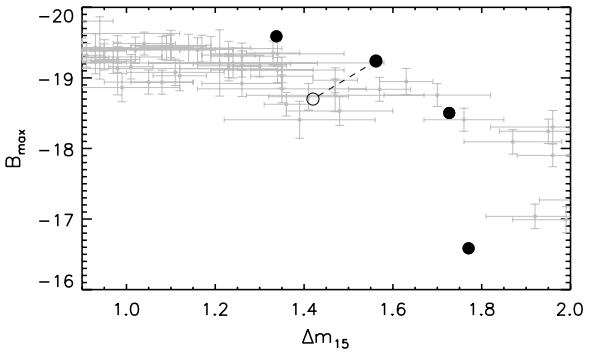

Figure 4. Comparison of the *B*-band light curve peak magnitude ($B_{\max}$) and decline-rate parameter (Δm_{15}) relation obtained from the models (solid circles) with observations of SNe Ia (Hicken et al. 2009; gray crosses). SNe Ia with distance modulus $\mu < 33$ have been excluded. The open circle shows the C+O+Ne model and is connected by a dashed line to the point for the pure-C+O model with the same $M_{\rm WD}$.

curves which decline more slowly. Compared to the observations the more massive models ($M_{\rm WD} = 1.06$ and $1.15\ M_\odot$) have Δm_{15} larger than observed for their brightness. We note, however, that Δm_{15} is a particularly challenging quantity to model precisely and systematic uncertainties in the radiative transfer simulations can affect this quantity significantly. For example, applying different radiative transfer codes to the well-known W7 model (Nomoto et al. 1984; Thielemann et al. 1986), which is widely regarded as a good standard for normal SNe Ia, yields Δm_{15} values that differ by several tenths of a magnitude (see, e.g., Figure 7 of Kromer & Sim 2009). Moreover, the values obtained are also too large compared to those of normal SNe Ia (e.g., ARTIS yields $\Delta m_{15} \sim 1.75$). The predicted width–luminosity relation is also affected by details of the initial WD as illustrated by our C+O+Ne test model. Compared to the equivalent pure-C+O model, this model declines more slowly in the *B* band and is fainter. This effect is sufficient to move this model to the opposite side of the observed width–luminosity relation (Figure 4). Thus, there may be potential for better agreement with observations from more detailed studies.

Finally, we note that the near-infrared light curves obtained from the models have characteristic features which are in qualitative agreement with observations of SNe Ia. For the brighter models ($M_{\rm WD} = 0.97$, 1.06, and $1.15\ M_\odot$), the *I*, *J*, *H*, and *K* light curves show distinct secondary maxima, while the faintest model ($M_{\rm WD} = 0.88\ M_\odot$) has single peaks. This is consistent with observations—normal SNe Ia show double-peaked near-infrared light curves, while sub-luminous events have single maxima (e.g., Wood-Vasey et al. 2008). Also, the difference between the models in the *J*, *H*, and *K* bands at *B*-band maximum light is much smaller than in the optical bands, consistent with the observation that SNe Ia are better standard candles at near-infrared wavelengths (Krisciunas et al. 2004).

6. DISCUSSION

The sub-$M_{\rm Ch}$ model for SNe Ia has much to commend it. First, it has already been suggested by empirical modeling of bolometric SNe Ia light curves (Stritzinger et al. 2006) that differing ejecta masses may be required for different SNe Ia, a property which the sub-$M_{\rm Ch}$ model may explain. Second, population synthesis studies predict large numbers of binary systems with accreting C+O WDs: Ruiter et al. (2009) estimate a Galactic rate of $\sim 10^{-3}$ yr^{-1} for possible explosions of sub-$M_{\rm Ch}$ C+O WDs accreting from helium-rich companions. This is much higher than their estimate of the Galactic rate for single-degenerate $M_{\rm Ch}$ explosions ($0.6–1.4 \times 10^{-4}$ yr^{-1}) and comparable to their estimate of the WD–WD merger rate ($1–2 \times 10^{-3}$ yr^{-1}) in systems that exceed $M_{\rm Ch}$. For comparison, the observed Galactic rate of SNe Ia is $(4 \pm 2) \times 10^{-3}$ yr^{-1} (Cappellaro et al. 1999).

Moreover, sub-$M_{\rm Ch}$ models provide a simple physical parameter which could account for the range of observed brightnesses: the mass of the exploding C+O WD. This parameter allows for a possible link between the typical brightness of an SN Ia and the stellar population in which it resides. For example, if it can be shown that explosions in binary systems with larger $M_{\rm WD}$ are more often found among young stellar populations relative to their less massive $M_{\rm WD}$ counterparts, the observed correlation of SN Ia brightness with host galaxy type (e.g., Howell 2001) might be explained.

Here we have shown that detonations of sub-$M_{\rm Ch}$ WDs lead to explosions which give a reasonable match to several properties of SNe Ia. Specifically, WDs with masses between $\sim$1 and $\sim 1.2\ M_\odot$ can reproduce a wide range of brightness with light curves that have rise times and peak colors in roughly the correct range. In addition, the models reproduce the characteristic spectral features present around maximum light and the observed trend for a higher velocity at the inner boundary of the IME-rich layer in brighter SNe Ia (Mazzali et al. 2007). Although our pure-C+O models yield light curves that fade too fast after maximum, the models predict a width–luminosity relation which behaves in the observed sense, and we argue that the combination of uncertainties in radiative transfer simulations and details of the nucleosynthesis (which is sensitive to the progenitor composition) can systematically affect the decline timescale. Thus, there is potential for even better agreement with improved modeling.

There are several additional observational constraints that our current models do not address but which should be considered in future studies. For example, off-center detonation might lead to observable effects associated with departures from spherical symmetry (e.g., Fink et al. 2010). Chemical inhomogeneity of the pre-explosion WD could affect the explosive nucleosynthesis: in particular, significant gravitational settling of ^{22}Ne (Bildsten & Hall 2001; García-Berro et al. 2008) might yield a layered ejecta structure with a central concentration of neutron-rich isotopes as favored by observations (e.g., Höflich et al. 2004; Gerardy et al. 2007).

In conclusion, detonations of naked sub-$M_{\rm Ch}$ C+O WDs yield light curves and spectra which are in qualitatively good agreement with the observed properties of SNe Ia. The critical question remains whether or not realistic progenitor scenarios in which the optical display is dominated by such an explosion can be established: it must involve detonation of a WD with a density profile similar to those of our toy models without producing large masses of high-velocity IGEs. Any sub-$M_{\rm Ch}$ scenario which meets these criteria will likely be promising in accounting for the observed characteristics of SNe Ia.

We thank S. Taubenberger for useful discussions and preparation of the observational data shown in Figure 4. This work was partially supported by the Deutsche Forschungsgemeinschaft via the Transregional Collaborative Research Center TRR33 and the Emmy Noether Program (RO3676/1-1). Simulations were carried out on the JUGENE supercomputer of Forschungszentrum Jülich.

REFERENCES

Arnett, W. D., Truran, J. W., & Woosley, S. E. 1971, ApJ, 165, 87
Benetti, S., et al. 2005, ApJ, 623, 1011
Bildsten, L., & Hall, D. M. 2001, ApJ, 549, L219
Bildsten, L., Shen, K. J., Weinberg, N. N., & Nelemans, G. 2007, ApJ, 662, L95
Bongard, S., Baron, E., Smadja, G., Branch, D., & Hauschildt, P. H. 2006, ApJ, 647, 513
Cappellaro, E., Evans, R., & Turatto, M. 1999, A&A, 351, 459
Conley, A., et al. 2006, AJ, 132, 1707
Domínguez, I., Höflich, P., & Straniero, O. 2001, ApJ, 557, 279
Fink, M., Hillebrandt, W., & Röpke, F. K. 2007, A&A, 476, 1133
Fink, M., et al. 2010, A&A, in press (arXiv:1002.2173)
Gamezo, V. N., Wheeler, J. C., Khokhlov, A. M., & Oran, E. S. 1999, ApJ, 512, 827
Garavini, G., et al. 2007, A&A, 471, 527
García-Berro, E., Althaus, L. G., Córsico, A. H., & Isern, J. 2008, ApJ, 677, 473
Gerardy, C. L., et al. 2007, ApJ, 661, 995
Guillochon, J., Dan, M., Ramirez-Ruiz, E., & Rosswog, S. 2010, ApJ, 709, L64
Hachinger, S., Mazzali, P. A., Tanaka, M., Hillebrandt, W., & Benetti, S. 2008, MNRAS, 389, 1087
Hicken, M., et al. 2009, ApJ, 700, 331
Höflich, P., & Khokhlov, A. 1996, ApJ, 457, 500
Höflich, P., Wheeler, J. C., & Thielemann, F. K. 1998, ApJ, 495, 617
Höflich, P., et al. 1996, ApJ, 472, L81
Höflich, P., et al. 2004, ApJ, 617, 1258
Howell, D. A. 2001, ApJ, 554, L193
Kasen, D., Röpke, F. K., & Woosley, S. E. 2009, Nature, 460, 869
Khokhlov, A. M. 1991, A&A, 245, 114
Krisciunas, K., Phillips, M. M., & Suntzeff, N. B. 2004, ApJ, 602, L81
Kromer, M., & Sim, S. A. 2009, MNRAS, 398, 1809
Livne, E., & Arnett, D. 1995, ApJ, 452, 62
Lorén-Aguilar, P., Isern, J., & García-Berro, E. 2009, A&A, 500, 1193
Mazzali, P. A., Röpke, F. K., Benetti, S., & Hillebrandt, W. 2007, Science, 315, 825
Nomoto, K., Thielemann, F.-K., & Yokoi, K. 1984, ApJ, 286, 644
Nugent, P., Baron, E., Branch, D., Fisher, A., & Hauschildt, P. H. 1997, ApJ, 485, 812
Nugent, P., Phillips, M., Baron, E., Branch, D., & Hauschildt, P. 1995, ApJ, 455, L147
Pastorello, A., et al. 2007a, MNRAS, 377, 1531
Pastorello, A., et al. 2007b, MNRAS, 376, 1301
Reinecke, M., Hillebrandt, W., Niemeyer, J. C., Klein, R., & Gröbl, A. 1999, A&A, 347, 724
Ruiter, A. J., Belczynski, K., & Fryer, C. 2009, ApJ, 699, 2026
Salaris, M., et al. 1997, ApJ, 486, 413
Shigeyama, T., Nomoto, K., Yamaoka, H., & Thielemann, F. 1992, ApJ, 386, L13
Sim, S. A. 2007, MNRAS, 375, 154
Stritzinger, M., Leibundgut, B., Walch, S., & Contardo, G. 2006, A&A, 450, 241
Thielemann, F.-K., Nomoto, K., & Yokoi, K. 1986, A&A, 158, 17
Travaglio, C., Hillebrandt, W., Reinecke, M., & Thielemann, F.-K. 2004, A&A, 425, 1029
Wood-Vasey, W. M., et al. 2008, ApJ, 689, 377
Woosley, S. E., & Weaver, T. A. 1986, ARA&A, 24, 205
Woosley, S. E., & Weaver, T. A. 1994, ApJ, 423, 371